Korean J. Chem. Eng., 38(7), 1333-1347 (2021)
DOI: 10.1007/s11814-021-0789-1

pISSN: 0256-1115
eISSN: 1975-7220

Multiscale modeling and integration of a combined cycle power plant and a two-tank thermal energy storage system with gPROMS and SimCentral

JaeHun Chang*, GunHee Lee, Derrick Adams*, HyungWoong Ahn***, JaeCheol Lee****,†, and Min Oh*,†**

*Department of Chemical Engineering, Hanbat National University, San 16-1, Dukmyung-dong, Yuseong-gu, Daejeon 34158, Korea
**PENTECH Engineering, 803, JEI PLATZ, 186, Gasan Digital 1-ro, Geumcheon-gu, Seoul 08502, Korea
***Institute for Materials and Processes, School of Engineering, The University of Edinburgh, Robert Stevenson Road, Edinburgh, EH9 3FB, UK
****AVEVA, 13F, Kbiz DMC Tower, 189, Seongam-ro, Mapo-gu, Seoul 03929, Korea
(*Received 16 December 2020 • Revised 26 February 2021 • Accepted 16 March 2021*)

Abstract−With different computational tools, simulations ranging from detailed and rigorous mathematical models to overall process plant of black box models can be carried out. Whereas most of these computational tools cannot practically execute different scales of models at the same time, it becomes relevant to devise strategies in coupling two or more of them for better analysis of processes. In this light, this study proposes Excel as an interactive scale bridge of data exchange to aid the multiscale modeling and dynamic simulation of combined cycle (CC) power plant integration with two-tank thermal energy storage (TES) system using gPROMS and SimCentral. This is relevant to analyze not only the performance of TES, but the feasibility of its integration with CC in augmenting energy production to meet daily power demand. The integrated system modeled in four operational modes of CC increased in power generation by 7.3 MW at an efficiency of 98.30%. The study validated the usefulness of the TES integration of 99.66% efficiency. The research results provide a communication strategy for different computational tools and an approach to effectively increase CC power production to meet varying daily demand.

Keywords: Thermal Energy Storage, Combined Cycle, Multiscale Modeling, Dynamic Simulation, Parametric Study

INTRODUCTION

The energy crisis has driven the pursuit of advanced technology for sustainable energy production. Global energy consumption is expected to increase by 55% between 2005 and 2030, while electricity use will double and coal consumption will increase by 73%. Three-quarters of this increase in energy consumption is expected in developing countries [1]. This has led to the search for other energy sources and renewable energy technologies, predominantly solar and wind. While new energy sources will be of significant contribution, there is the need for smarter ways to efficiently utilize existing energy systems to increase production. According to electric power statistics, the demand during the day is higher as compared to the night [2], and thus it is relevant to save energy, especially from unvarying power plant systems.

Power generation systems generally consist of nuclear power, combined heat and power (CHP), combined cycle (CC) power generation, and oil power generation. They are characterized as either base load or peak load power plants according to their application. Whereas power plants for base load operations produce constant electricity, the peak loads are dispatched to augment base loads in times of high electricity demand. For instance, Germany, South Korea, United Arab Emirates, Mexico, and the United States of America use peak load power generation plants for reasons of outstanding performance, high availability and operation flexibility, whereas base load power plants are used in countries such as Iceland, Russia and Taiwan for reasons including, but not limited to, reliability and cheapness to operate [3]. CC and CHP offer the flexibility for both base and peak load operations, which are adopted for reasons stated earlier in countries that use them. However, the base load operation does not always imply the maximum power capacity of the plant itself, but it is related to the economics of production. Hence, the motivation to consider ways to recover excess thermal energy from base load operations to use during increasing demand at peak loads.

Thermal energy storage (TES) technologies have been proven in several studies as feasible conjunction with most of the power generation systems. The potential benefits of this integration have been captured in [4,5]. Among the TES technologies, research into two-tank system using molten salt has gained more interest. It is mostly used in concentrating solar power (CSP) plants of base load and peak load operations to store energy. Despite the laudable advantages over its counterparts (PCM, thermocline storages, sorption heat storages etc.) further research in understanding salt freezing behavior in the tank, heat loss control, optimizations and others, need to be considered [6]. Some studies of the integrated process using TES have been summarized in Table 1, which are grouped into 1) performance and economic analysis of CSP [7-9]; 2) TES

†To whom correspondence should be addressed.
E-mail: jc.lee@aveva.com, minoh@hanbat.ac.kr

Table 1. A literature review of TES systems

Researchers	Major assumptions and results
Isabel Liorente et al. [7]	- Two-tank TES system using molten salts of Sodium and Potassium nitrate. - 50 MWe CSP plant is presented and compared to real data from an equivalent power plant currently operated by the ACS industrial Group in Spain using Wolfram's Mathematica 7. - Simulation result showed that the gross electrical power generated could vary around 2-3%.
C. Parrado et al. [8]	- An economic analysis was carried out for computing projection of levelized cost of energy (LCOE) between 2014 and 2050 from a 50 MW CSP plant with five different compositions of molten salts consisting of lithium, sodium, potassium nitrates and calcium. - $48\%Ca(NO_3)_2+7\%NaNO_3+45\%KNO_3$ was proposed as a new molten salt, which could reduce the storage costs in CSP plants. - The LCOE of CSP plant with the new molten salt in the Atacama Desert showed almost a 47% and 30% lower cost than south of Spain and California, respectively, during the projection period.
Lukas Heller et al. [9]	- CC CSP plant with thermocline-based rock bed TES was simulated using MATLAB. The calculated LCOE is in the range of 0.11-0.18 EUR/kWh. - The concept of a CC CSP plant with a thermocline-based rock bed TES system showed promising results. This storage system technology has, however, not yet proved feasible for CSP and thus further development of the technology is required.
Daniel Curtis et al. [10]	- The methodology of six TES technologies (*e.g.*, steam accumulator TES, packed-bed TES system, sensible heat (SH) TES, hot rock TES, geologic TES and cryogenic air TES) have been qualitatively analyzed for the deployment and operation of integrated TES with NPP. - NPP with integrated TES has three main modes of operation available: base-load, charging and discharging. - Integration of TES into both existing and new NPP offers a plausible option to improve competitiveness by simultaneous flexible electricity output and constant full power operation of the nuclear core.
Jacob Edwards et al. [11]	- Exergy analysis for viability examination was performed for a light-water-cooled NPP with four different types of TES materials; Nitrate salt with Denstone-99 Alumina as active TES, Therminol-66 and Dowtherm-T as passive TES. - The conclusion was that the exergetic efficiency of active type is 92-93%, and the passive type is 77-78% when merged with NPPs.
Vasilios Vamvas [17]	- This patent suggested five configurations of CC power plants consisting of a gas/steam turbine, heat recovery steam generator (HRSG), TES and retrieval system charged by solar thermal power. For latent heat (LH) TES, phase change materials receive thermal charge from solar energy and GT exhaust heat. TES system provides supercritical steam. - This researched the application of a single stage and two stage LHTES in a CC power plant. The results concluded that two-stage LHTES is more highly effective than single LHTES in view of thermal efficiency.
Kevin Drost et al. [18]	- Examined the feasibility of TES system using molten nitrate salt with a 500 MW Class IGCC power plant to efficiently provide peak and intermediate load electric power. - IGCC with TES system has the potential to minimize the cost of electric power of peak and intermediate load by 5-20% based on operating conditions of plant. - Developed molten salt TES technology; several advanced concepts such as direct contact salt heating, low freezing point salt and advanced tank designs require research and development.
M. K. Drost et al. [19]	- Discussed the technicalities and evaluated the economics of molten nitrate salt TES system integration with IGCC power plant. - During peak demand periods, the TES system supplies additional energy to produce 538 °C and 16.5 Mpa superheated steam. - The results indicated that IGCC - TES system integration can minimize the cost of peak and intermediate electric supply by at most 20% comparing to other coal-fired power plants.
Bandar Jubran Alqahtani [13]	- Simulated a 50 MW CSP using molten salts with NREL System Advisory Model (SAM) for performance analysis and 500 MW NGCC plants with MATLAB. - Reported that ISCC plant is more economical than NGCC for gas prices ranging from 9.5-10.5 $/MMBtu even at no subsidies.
Oliver Garbrecht et al. [14]	- Used EBSILON to analyze the integration of a 300 MW fossil-fired power plants and molten salt TES system. - Simulation result showed that total operating time is 87 minutes: 15 min for discharging (319 MW), 10 & 62 min (293 and 298 MW) for the two charging modes. - The authors suggested further studies to assess the investment returns of this project.

Table 1. Continued

Researchers	Major assumptions and results
M. Johnson et al. [15]	- The temperature of the nitrate salts used as the phase change material (PCM)s ranges from 140 °C to 350 °C. - Outlined the method for designing an LHTES unit for turbine failure in the cogeneration plant. The secondary boiler produces steam at 25 bar, 300 °C, while the TES system is able to generate 6 MW power for 15 minutes in case of turbine failure.
Prashant Verma et al. [16]	- Thermo-physical properties of 13 inorganic and 9 organic PCMs were scrutinized for LHTES system employment. - Mathematical modeling of two types of LHTES (*e.g.*, cylinder-packed vessel and rectangular container) was considered using the thermodynamic (first and second) laws in FORTRAN code. - The authors suggested further experimental examination to validate the first and second law analysis.

application methods and exergetic analysis for nuclear power plants (NPP) [10,11]; 3) performance and technical analysis of integrated gasification combined cycle (IGCC) [12]; and 4) technical and thermodynamic analysis of CHP, natural gas combined cycle (NGCC) and fossil fuel power plants [13-15].

Apart from what has been mentioned above, it is interesting to note the possibility of applying a multiscale modeling approach to a combined cycle power plant and TES system. While it may not be an exaggeration to say process systems are inherently multiscale, simulation of such systems is mainly of length and time scales phenomena at different levels. A previous study classified two numerical simulation approaches in handling multiscale problems: global governing equations for the entire domain and sectional modeling at different scales with communication at their interfaces [20].

In this sense, devising an advanced computational technique [21] would not only be beneficial to understanding the behavior of the CC integration with the TES system, but it would help apply this approach for theoretical study in process modeling and simulation.

However, there have been a few studies in multiscale modeling of TES. Furthermore, none of them has been found in the open literature on two-tank heat storage with molten salt. Helmns et al. [22] established a framework of multiscale design to assess the performance model of phase change material (PCM) TES integrated with subsystem heat exchanger. To overcome a slow charging rate of paraffin wax in a shell and tube TES unit, previous studies adopted a multiscale heat transfer enhancement technique [23]. On the other hand, a hybrid molecular dynamics and Monte Carlo method were implemented to investigate materials for sorption heat storage (SHS) in a multiscale simulation [24]. These studies mainly focused on the material for the TES system.

Considering the relevance of multiscale modeling and simulation in chemical, environmental and process engineering, the coupling of different computational tools to model and optimize processes, as well as systems, presents challenges which have gained research interest. Merging of several systems such as model development (ModDev), modeling tool (MoT) and ICAS with the aid of COM-Objects or CAPE-OPEN [25] has been successfully applied in product and process design [26]. Further development established a framework for different computational tools with multiscale features to provide systematic work and data flows for several design problems [27]. With the same CAPE-OPEN standard interfaces, Simulis Thermodynamics and ICAS modeling tools were integrated for the computation of thermodynamic properties using standard middleware (DLL file) as the medium for interconnectivity [28]. In addition, the idea of multiscale modeling for product manufacturing of chemical reactor has been explored. On the different scales of length and time, the computational tools such as process system modeling, computational fluid dynamics and computational chemistry were integrated using the CAPE-OPEN interface to enable data exchange between the different tools [29].

For structured reactors, a multiscale strategy has been employed in the design and optimization of a hierarchical model where results are transferrable across models for pressure drop coefficient approximation [30]. Also, a multiscale framework has been developed for the production of hydrogen by the decomposition of ammonia on ruthenium as well as a parameter estimation model to optimize reactions [31]. Concerning computations, a multiscale method was implemented to significantly decrease the computational time of a three-phase flow configuration where a dual-grid approach was used to handle information between two scales [32]. In the development of a multiscale packed model of carbon dioxide absorber and stripper, an enhancement factor calculated from the microscale model using concentration profiles of chemical species was incorporated into macroscale computations for unit design [33].

The aforementioned studies have explored multiscale modeling and simulations from different perspectives, achieving varying success. However, none to our knowledge has conducted a dynamic simulation with different platform integrations to study a process behavior particularly TES and CC at different scales. A major issue of this is the difficulty in connecting them dynamically without being out of synchronization in time during the simulation. Thus, in this study we 1) developed a multiscale model that dynamically bridges macroscale combined cycle power plant model in SimCentral with mesoscale TES model in gPROMS using Excel interface as a communication medium, 2) examined the potential of combined cycle integration with TES, and 3) analyzed the energy storage performance of the TES in meeting daily power demand. The novelty of this research presents a unified multiscale framework with a developed Excel interface other than popular CAPE-OPEN for dynamic simulation. In particular, the combined cycle simulation with SimCentral outlines the performance of the plant at four operational modes, while the gPROMS [34-37] helps to assess TES efficiency.

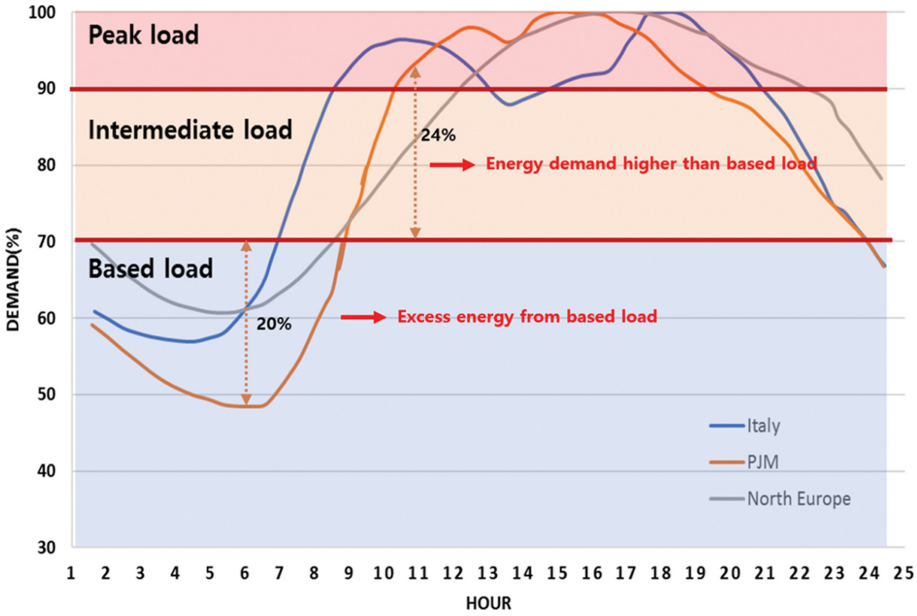

Fig. 1. Global power demand in a day for three countries showing their various loads: PJM is the US electricity market [38].

PROBLEM FORMULATION

As electricity is produced, it is concurrently consumed. This is a characteristic of electricity that presents issues of stability and quality when there is a disparity in demand and supply of power. Therefore, it is very important to maintain balance at varying demand. As seen in Fig. 1, power demand varies from time to time and so does its price due to the cost of production. During high demand for power that is peak period, supplementing base load power plants becomes necessary, which comes at a higher cost from the power suppliers than the average demand. Instead of augmenting with another power generation system, the approach of storing electricity during the night time and reinserting it during the peak periods offers a huge potential to reduce the total generation cost. From Fig. 1, energy usage is far below the baseline supply between the hours of 1 and 9 for all the load curves and higher from hours of 9 to 23. Hence, storing the excess energy during low demand hours at base load operations can be used to augment the higher demand at peak load. For example, the base load operation provides about 22% excess energy supply with reference to the actual demand at the 6th hour on the PJM load curve and about 25% less at the 11th hour during peak load. With the concept of this study, the excess energy of the base load operation at the 6th hour can be stored and used at the 11th hour to increase the 70% baseline supply to about 80%. This study thus proposes a combined cycle (CC) power plant with thermal energy storage (TES) for this implementation.

1. Performance Analysis

Typically combined cycle power plants consist of a gas turbine and a steam turbine which operate under the thermodynamic cycles of Brayton and Rankine, respectively. After completing the first

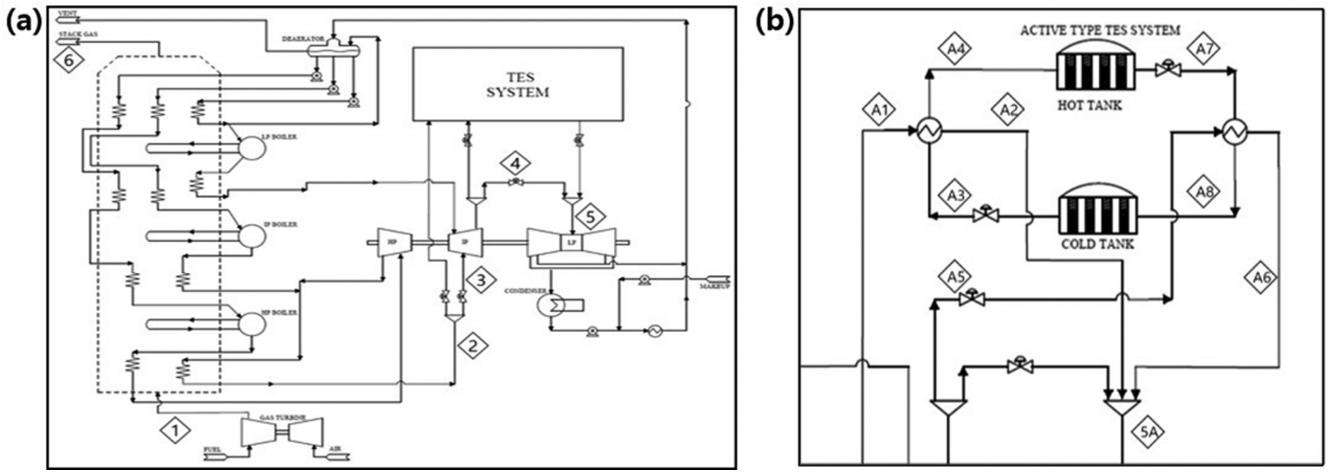

Fig. 2. Schematic diagram of combined cycle with TES system and detailed unit processes: (a) Combined cycle with TES, (b) two-tank TES system.

cycle (Brayton), the high temperature working fluid that would have escaped through the exhaust is captured by a heat recovery steam generator (HRSG) to generate steam. The steam is then released to the steam turbine (second cycle) for additional power generation, and the low-temperature liquid ends up in the condenser where it is recycled to start the whole combined cycle.

The TES system is a two-tank storage unit with molten salt as the thermal storage material (TSM) designed to store excess energy during low demand of power for later use. It consists of a hot and cold tank to hold molten salt at high and low temperature, respectively. To this purpose, they are well insulated to minimize the loss of heat to the environment.

2. Multiscale Modeling of Unified Framework

There are various computational tools for modeling and replicating chemical engineering processes. Of these are process simulators capable of simulating mathematical models of different order of magnitude in the spatial and temporal scales. The complexity of these mathematical models requires sophisticated computational strategies to carry out the simulations. Hence, multiscale modeling becomes relevant not only to replicating the physical processes but offering insights into the real behavior of the process units.

In the multiscale computing environment, the concept of multiscale modeling has a few unresolved questions, although it is largely used in most fields of science. The questions range from terminology to general approach or technique in modeling a multiscale system and computations. There are different schools of thought among researchers in different research communities, basically because of how multiscale is perceived. Interestingly, the terms used in these fields could mean the same thing, while others may be quite different based on the field.

However, there are a few researches [39-42] with a methodological approach to the multiscale concept. In pursuit of common grounds on multiscale modeling [43,44], proposed a possible approach. The authors formulated a multiscale modeling and simulation framework which defines multiscale as a group of single-scale models interconnected through a modeling language or scale bridging methods. These bridging methods are the heart of multiscale modeling, especially when different computational tools are involved in its simulation. Popular among the computational community in chemical engineering over the years is CAPE-OPEN.

While CAPE-OPEN standard interface in combination with other processes [26,27,45] has achieved great results, its challenges cannot be overlooked. This study sought an alternative in coupling meso-macro scales of different computational tools for dynamic simulation. We leveraged the visual basic option in Excel, a common and easy-to-use software as the communication channel between the different scales of gPROMS and SimCentral for dynamic simulation, which is not found in any research field. Not only was the data exchange feasible, but there was no spike in computational demand for the multiscale unified framework simulation [43,44]. gPROMS and SimCentral computational tools used in this study are capable of modeling and simulating processes in steady and dynamic states. gPROMS comes with a wide scope of numerical solvers for detailed mathematical modeling of process systems ranging from zero to two dimensions where numerical analysis of partial differential-algebraic equations can be handled. SimCentral, on the other hand, provides the flexibility to carry out process simulations roughly from a unit process to an entire process like Aspen plus, Pro II and others. It is widely used in the chemical engineering community for dynamic simulation.

3. TES Modeling Approach

TES is a technology widely employed to store excess thermal energy and used at later times. The technology ranges from different concepts on how the energy is stored and the kind of materials used. Among the TSMs, molten salt is used due to its high energy capacity storage from sensible heat. This study thus used it to balance the hourly supply and demand for energy in the CC operations. It was the mesoscale model for the CC integration simulation which provided internal insights into the dynamic behavior of heat loss during operation. As the TES interacts with the CC during simulation, the hot tank section charges for three hours during excess production at base load operation, stores high-temperature TSM for six hours, release the energy to the CC for eight hours during peak load demand and then the low-temperature TSM return to cold tank section, which takes seven hours. During storage periods in the hot and cold tanks, the gPROMS simulation provides

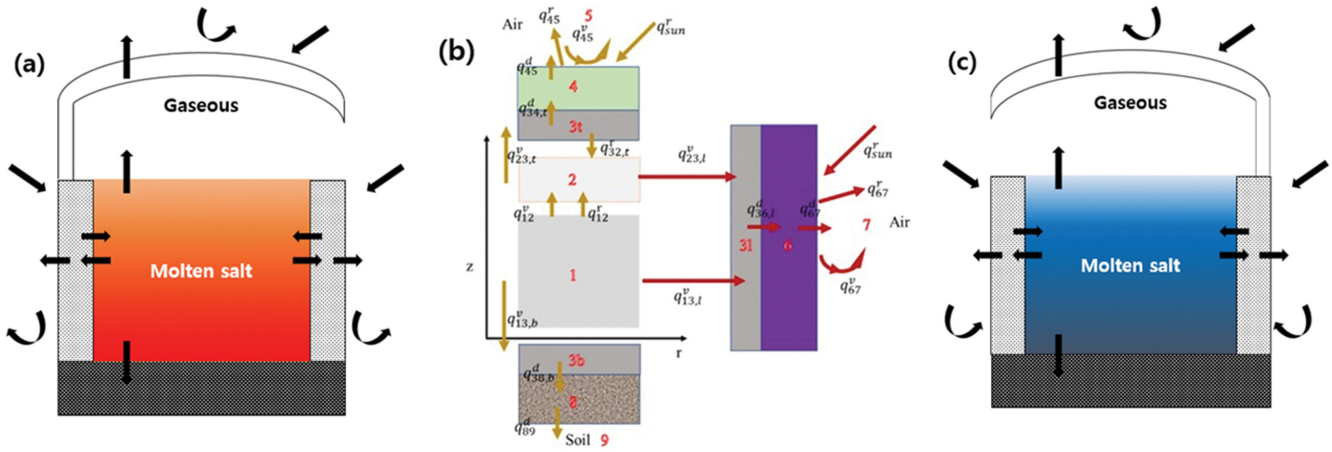

Fig. 3. Molten salt two-tank thermal energy storage system – heat flows influenced by temperature gradient. (a) Hot tank, (b) schematic diagram of heat transfers, (c) cold tank.

the rate of heat loss through the various sides of the tank as well as during charging and discharging to the CC with the SimCentral. The hot tank part of the TES can be modeled as the mirror image of the cold tank for the integrated system simulation.

The gPROMS ProcessBuilder chosen for the mesoscale modeling of the two-tank TES system is an advanced process environment that enables one to build models, validate and execute steady-state and dynamic simulations. By sectioning the whole storage tank into submodels, the basic models of heat transfer such as conduction, convection and radiation were used to evaluate the high-temperature molten salt tank exposed to the surroundings.

The modeling of the tanks shown in Fig. 3 followed the methodology proposed by Zaversky et al. [46]. Fig. 3(a) and (c) are the hot and cold tanks, respectively, which shows the heat transfer inside the tank and with the surroundings. Since the temperature inside the two tanks is higher than the surroundings, heat loss is expected through the mechanism, as shown in Fig. 3(b). The molten salt, molten salt composition (60% $NaNO_3$ and 40% KNO_3), which is the most used sensible heat TSM in solar power plants, was chosen for this study considering its wide range of temperature making it suitable for the combined cycle power plant operating temperature. Full properties can be found in Table 3. The molten salt exchanges heat via convection with the inner walls of the tank, bottom, the atmospheric gas and the surrounding.

With the sub-models, the study considered transient behavior of the molten salt (1), tank's atmospheric gas (2), tank walls (31) and insulation (6), the roof (3t) and insulation (4), different materials of the bottom (3b, 8, 9) and the tank surroundings (5,7). The molten salt as well as the atmospheric gas region can be evaluated with the global mass and energy balances taking into consideration its interaction with the sub-models at their interfaces. One dimensional conduction heat transfer of multiple material layers was modeled for the tank roof, walls and the bottom. The wall was modeled as cylindrical while the roof and the bottoms as planar conduction heat transfers. On the interfaces where the sub-models interact, convection models between the molten salts, tank walls, roof, bottom, atmospheric gas and the tank surrounding were considered. Also, the radiation models were evaluated between the atmospheric gas, unwetted walls, roof, molten salt and the surroundings. These make the complete mesoscale model of the TES tank, which is computed with the gPROMS advanced tool.

The mathematical description of the TES storage unit is presented in Table 2 based on the assumptions mentioned above. The mass and energy balance (Eq. (5) and Eq. (6)) include time derivatives, which are differential equations. On the other hand, the heat source terms, Eq. (7) and heat transfer equations Eq. (8)-Eq. (18) are algebraic equations. Since Eq. (9), Eq. (13) and Eq. (14) are nonlinear terms, the resulting equations are a set of nonlinear differential-algebraic equations (DAEs). By gPROMS solving approach, this can be represented by the below equations [47].

$$f(x', x, y, t) = 0 \tag{1}$$

$$g(x, y, t) = 0 \tag{2}$$

where x and y are n and m dimensional vectors of variables,

Table 2. Rigorous conservation and other closure mathematical modeling for TES system

Description	Mass/Energy transfer type	Formula	
Molten salt model	Mass balance	$\frac{dm}{dt} = (\dot{m}_{in} - \dot{m}_{out})$	(5)
	Energy balance	$\rho c_p V \frac{dT}{dt} = \dot{m}_{in} \cdot \bar{h}_{in} - \dot{m}_{out} \cdot \bar{h}_{out} + Se$	(6)
		$Se = q^{v}_{12} - q^{\Re}_{12} - q^{v}_{13,l} - q^{v}_{13,b}$	(7)
		$q^{v}_{ij} = h_i A_i (T_j - T_i)$	(8)
		$q^{\Re}_{ij} = \sigma A_i \varepsilon (T_i^4 - T_j^4)$	(9)
		Conduction=d: $q^{d}_{ij} = \frac{k_i A_i}{l_i}(T_i - T_j)$	(10)
		Convection=v: $q^{v}_{ij} = h^{v}_i A_j (T_i - T_j)$	(11)
		Radiation=$\Re$: $q^{\Re}_{ij} = \sigma A_j \varepsilon (T_i^4 - T_j^4)$	(12)
		$R^{d}_{ij} = \sum_{ij}^{n} \ln\left(\frac{r_j}{r_i}\right)/(2\pi k_i l_i)$, $R^{\Re}_{ij} = \sum_{ij} \frac{1}{2\pi h^{v}_i r_j l_i}$, $R^{\Re}_{ij} = \frac{1}{2\pi h^{r}_i r_j l_i}$	(13)
		$h^{\Re}_{ij} = \varepsilon\sigma (T_i + T_j)(T_i^2 + T_j^2)$	(14)
Lateral side 1→7 2→	*Through the vertical walls to the outside*	$q_{17} = q^{v}_{13,l} + q^{d}_{36,l} + q^{d}_{67} + q^{v}_{67} + q^{\Re}_{67} - q^{\Re}_{sun}$	(15)
		$q_{27} = q^{v}_{23,l} + q^{d}_{36,l} + q^{d}_{67} + q^{v}_{67} + q^{\Re}_{67} - q^{\Re}_{sun}$	(16)
Topside 1→5	Inside the tank *Through the tank's top surface*	$q_{15} = q^{v}_{12} + q^{\Re}_{12} + q^{v}_{23,rf} + q^{d}_{34,rf} + q^{d}_{45} + q^{\Re}_{45} + q^{v}_{45} - q^{\Re}_{32,rf} - q^{\Re}_{sun}$	(17)
The bottom side 1→9	Inside the tank *Through the bottom insulation into the soil*	$q_{19} = q^{v}_{13,b} + q^{d}_{38,b} + q^{d}_{89,b}$	(18)

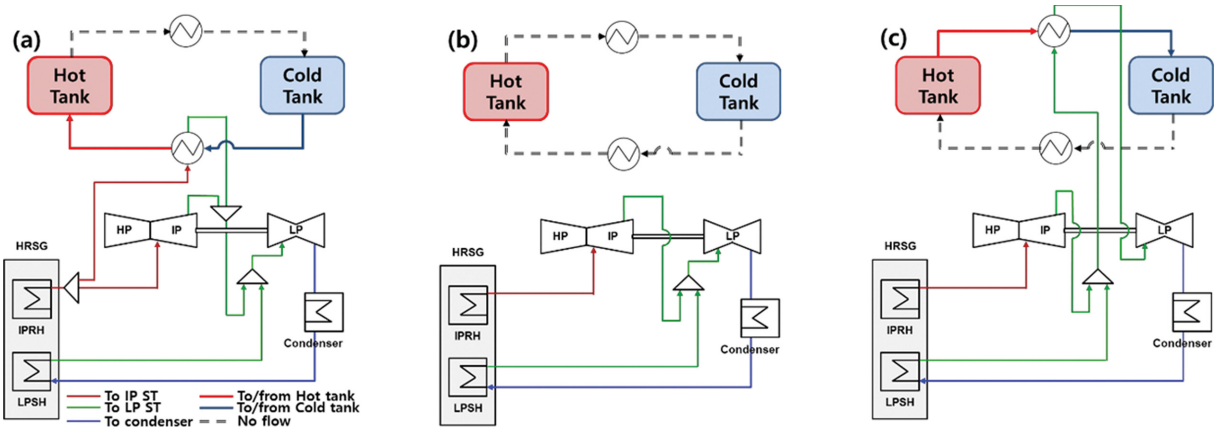

Fig. 4. Schematic diagram of CC with two-tank TES illustrating the different operation modes: (a) Charging mode, (b) storing or nomal mode, (c) discharging mode.

respectively, t is the independent variable and x′ is the derivative of x with respect to t. f and g are n and m dimensional systems of equations.

In gPROMS, the backward differentiation formulae (BDF) were employed with a predictor and corrector step to solve the DAEs described in Table 2. The k-step BDF method on the n^{th} integration step can be represented as [47]:

$$x'_n = \frac{1}{h_n \beta_k}\left(\alpha_k x_n + \sum_{j=0}^{k=1} \alpha_j x_{n+j-k}\right) = \frac{1}{h_n \beta_k}(\alpha_k x_n + \gamma_{k,n}) \quad (3)$$

where h_n is an integration step length, α_k, β_k are BDF coefficient and $\gamma_{k,n}$ is the accumulation of history terms in the BDF method. When this is substituted into the DAEs Eq. (1), the equation system becomes

$$f\left(\frac{1}{h_n \beta_k}(\alpha_k x_n + \gamma_{k,n}), x_n, y_n, t_n\right) \quad (4)$$

This is a set of nonlinear equations, which can be solved using Newton's family method. To obtain accurate solutions, absolute and relative tolerance were set to 10^{-5} in the gPROMS software for simulation.

Since the hot and cold tanks work in reverse to each other at every mode, as explained in section 2.4, the mathematical models governing their behavior are similar as provided in Table 2 except for the rate of flow. Refer to [6,46] for a detailed explanation.

4. Operation Scenario of Combined Cycle with TES

The operation modes of the integrated system are shown in Fig. 4(a) charging mode, (b) normal/Storing mode, (c) discharging mode. Each line in Fig. 4(b) can be adjusted to normal, charging, discharging, and storage modes. And Mode (a)/(b)/(c) are manipulated by flow control of heat source.

(a) Thermal charging mode: Low-temperature TSM from the cold tank gains heat by transfer from part of the steam flowing into IP ST through the heat exchanger and is stored in the hot tank. The resulting low-temperature steam is transported to the LP ST.

(b) Normal/storing mode: In these operation modes, there is no heat exchange between the CC and TES system since the full steam is utilized by the steam turbines. However, in normal mode, TSM is held in the cold tank, whereas in the storing mode, the high temperature TSM charged by the steam is stored in the hot tank.

(c) Discharging mode: High-temperature TSM from the hot tank augments the energy capacity of the steam from the IP ST through heat exchanger before it is transported to the LP ST. This increases the power generation of the steam turbines and the resulting low-temperature TSM is stored in the cold tank.

SOLUTION STRATEGY

1. Simulation Basis

The physical properties of the TSM used in this study are shown

Table 3. Properties of molten salt used as cold and hot thermal storage material [49,50]

Type	Active type
Components	60% $NaNO_3$-40% KNO_3
Freezing temperature (K)	493
Stabilizing temperature (K)	873
Density (kg/m^3)	1,899
Viscosity (cP)	3.26
Specific heat (J/kg-K)	1.495
Heat of fusion ((kJ/kg)	n/a

Table 4. Modeling and simulation basis for combined cycle with TES system [48,51]

System	Modeling basis	Value
TES	Thermal saving and adiabatic efficiency	99%
GT	Adiabatic GT efficiency	89%
	Pressure ratio	19.37
	Turbine inlet temperature	1,690.3 K
	Turbine outlet temperature	1,117.5K
ST	Adiabatic HP ST efficiency	92%
	Adiabatic IP ST efficiency	91%
	Adiabatic LP ST efficiency	93%

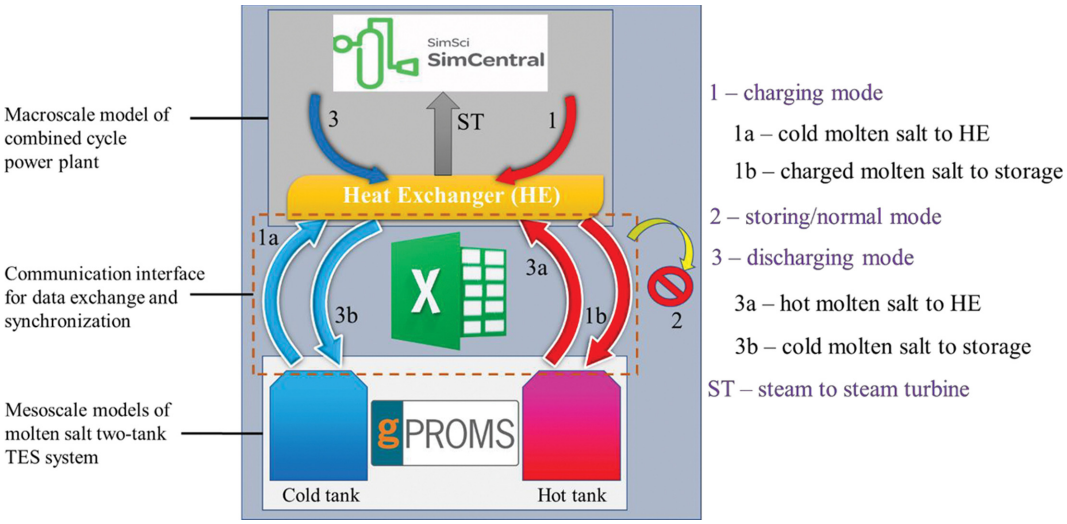

Fig. 5. Unified framework showing how the excel interface communicate with the macroscale model in SimCentral and mesoscale model in gPROMS at the various operations modes.

in Tables 3 and 4, which are the modeling basis of CC with the TES process. The modeling basis is referenced from CC's NETL report [40] to ensure reliability and validity. In addition, the thermodynamic model used in this study assumed an incompressible fluid for TSM with the SRK state equation, which is widely used for hydrocarbons.

2. Strategy for Multiscale Modeling of the Unified Framework

The SimCentral software is capable of steady and dynamic simulation. However, since the process simulator is a black box model, which is usually applicable to integrated processes, developing a detailed model for heat loss analysis of the TES system is a limitation. With the aid of gPROMS software, a detailed mathematical model of the TES was developed and simulated simultaneously with the SimCentral software where data are exchanged.

While the SimCentral model of the combined cycle with the TES system integration performed dynamic simulation under four operating conditions, the gPROMS analyzed the thermal efficiency of the two-tank TES. In addition, the Excel interface for the data exchange was constructed to enable the time synchronization and co-simulation of the two simulators for the multiscale model. The dynamic simulation was carried out at a 1-second interval in the two dynamic simulators.

The execution strategy of multiscale modeling and the dynamic simulation implemented in this research as shown in Fig. 5 is as follows.

- In charging mode, the steam flowing to the ST in the SimCentral model splits into two where one goes to the TES system. This steam stream (1) exchanges heat with the cold molten salt (1a) which gets charged (1b) and is stored in the hot tank. In the meantime, the Excel interface is set online enabling the transfer of TSM properties from SimCentral to gPROMS simultaneously for heat loss analysis. The resulting steam to the ST goes to the IP ST at a reduced temperature due to heat loss.
- The storing mode generates power in the same capacity as the normal mode in SimCentral. At these modes, the Excel connection is set offline. In the meantime, SimCentral simulates the macroscale model of the CC while gPROMS analyzes the rate of heat loss of the TS in the tank. At storing mode, the charged molten salt is held in the hot tank and at normal mode, the low-temperature molten salt is kept in the cold tank.
- In discharging mode, the power generation capacity of the plant increases as the steam flowing into the ST gains energy from the molten salt (3a) through the heat exchanger and the resulting molten salt (3b) is stored in the cold tank. While the heat exchange takes place, the Excel interface comes online to enable the communication between SimCentral and gPROMS for the dynamic simulation. In this mode, the resulting steam flowing to ST goes to LP ST in the SimCentral model.

This co-simulation of an integrated system provides insight into the behavior of the plant at different spatial and temporal scales. While the SimCentral model offers an overall dynamics of the system, the gPROMS helps to zoom into the behavior of the TES at a detailed level in terms of how the heat is lost and which part contributes the most of the losses. This can be applied to simulations of complex processes where one is interested in the detail dynamics of a certain unit. However, this can be of a huge computational burden as well as time lag when several individual units are to be modeled together.

RESULT AND DISCUSSION

1. Process Flow Diagram of CC with TES Based on the Unified Multiscale Framework

Fig. 6 shows the process flow diagram of CC with TES in SimCentral. The integration process enabled SimCentral software to perform dynamic simulation of CC and TES for four different operational modes (see Fig. 4). The process includes the main equipment (GT, ST, TES) shown in Fig. 2. The TES system was modeled to accept values from gPROMS via the black box system in SimCentral.

Fig. 7 shows a close view process flow diagram of the two-tank

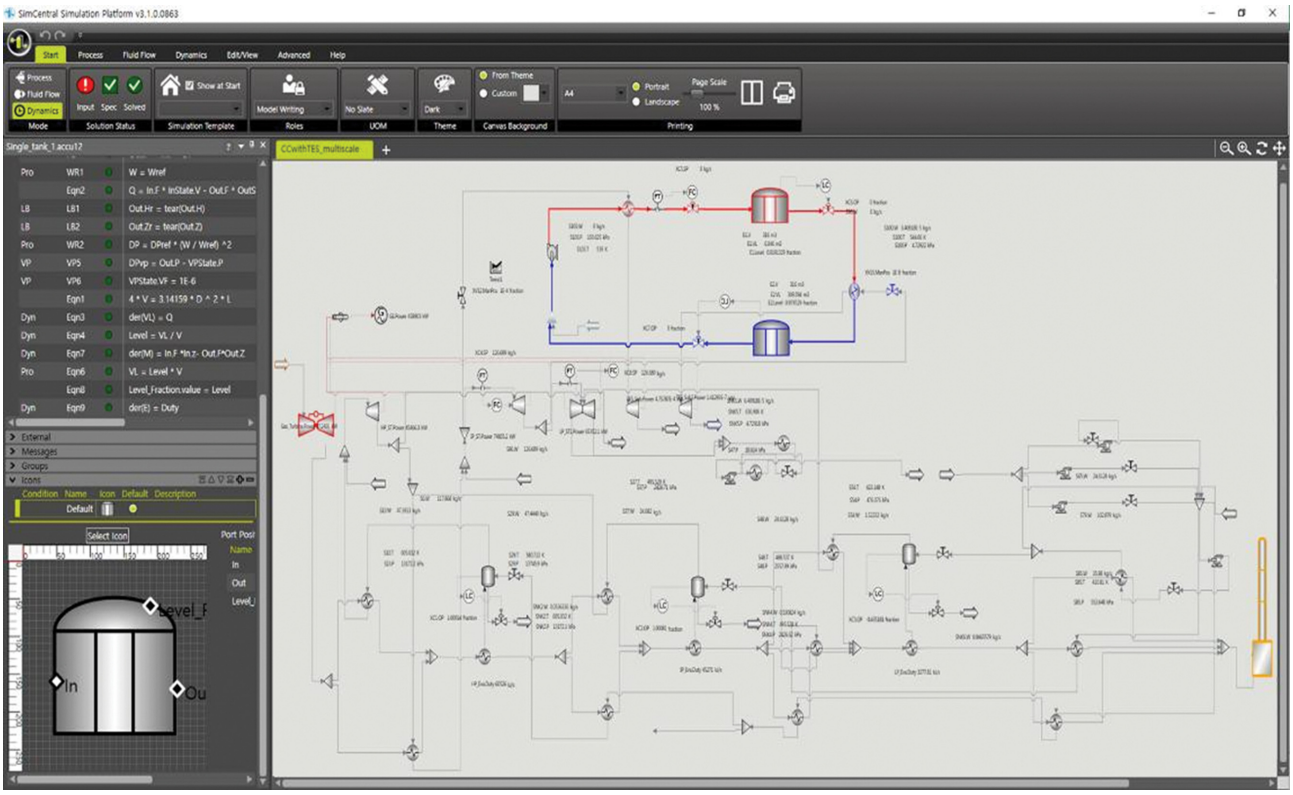

Fig. 6. Integrated combined cycle with a two-tank TES system process flow diagram. A strategy to deal with varying daily power demand.

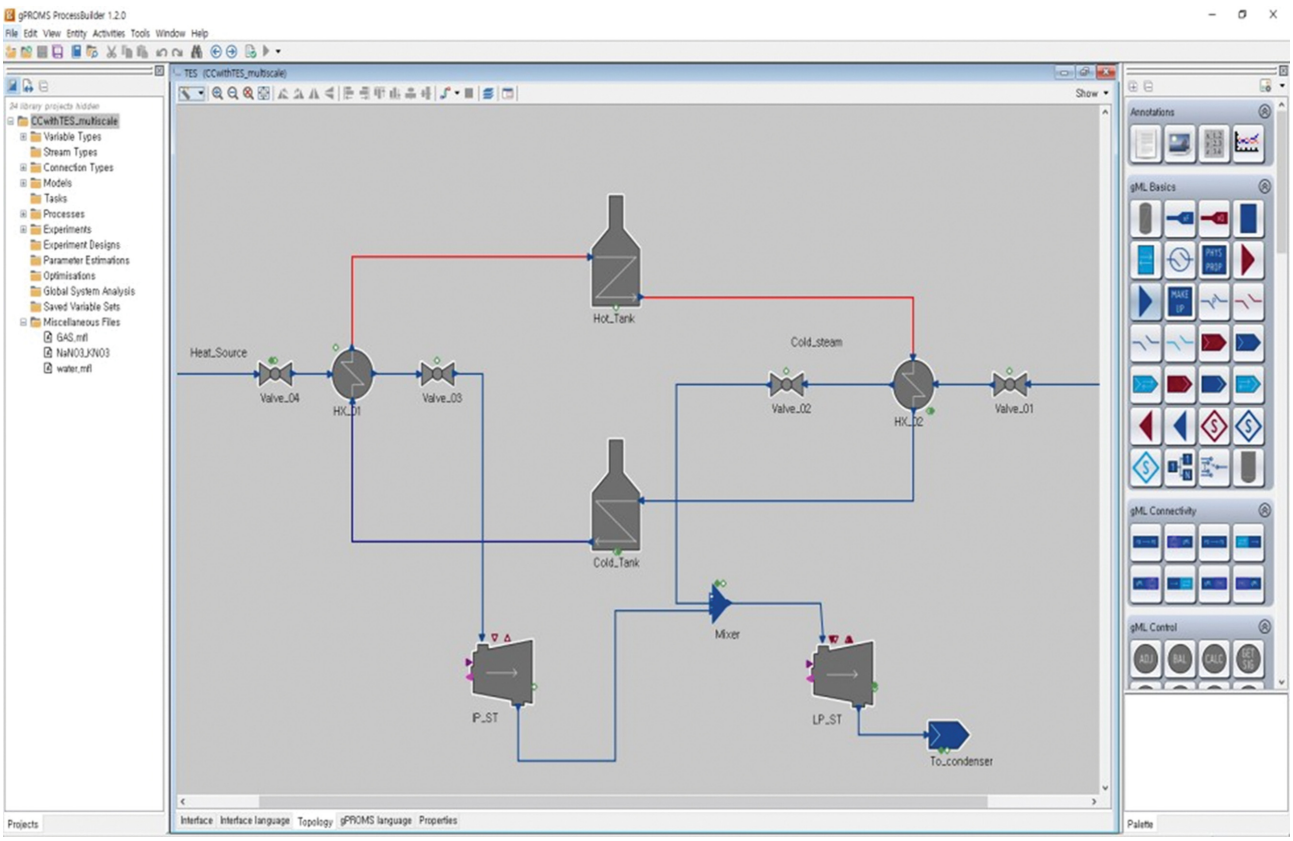

Fig. 7. gPROMS simulator for two storage TES tank process flow diagram within detailed mathematical modeling.

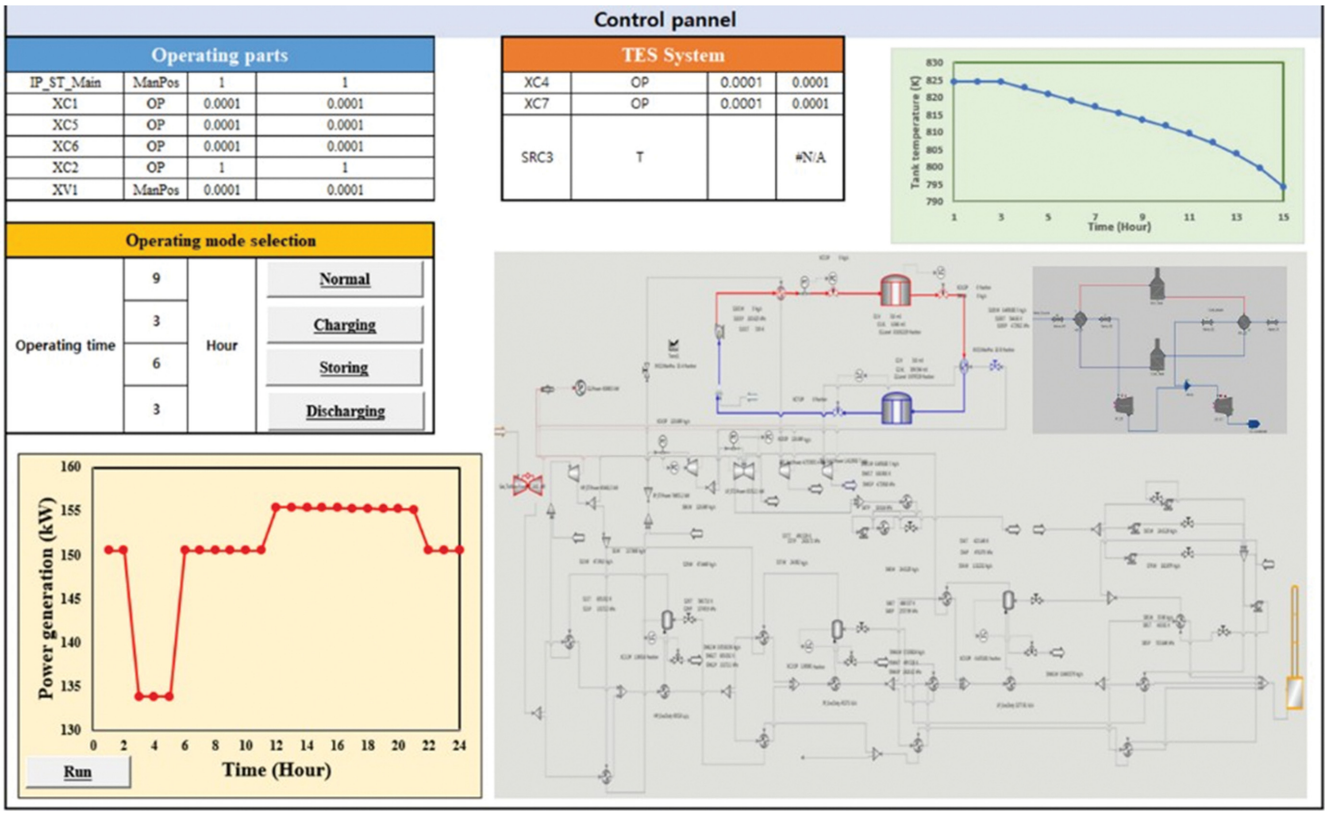

Fig. 8. Excel graphic user interface and dynamic control panel as a scale bridge for data and time synchronization between SimCentral and gPROMS simulator.

TES system. Its performance was analyzed through detailed mathematical modeling of mass and energy conservation laws and heat transfer using the gPROMS software. The framework was able to send and receive data such as steam and TSM flow rate, temperature between the integrated system. While these properties change at the various operating modes, the integrated system is configured for time synchronization to enable smooth communication in the dynamic simulation.

Fig. 8 shows the Excel interface developed to serve as a scale bridge for the multiscale modeling and simulation of CC with TES. In the Excel interface, SimCentral and gPROMS exchange data in the same time zone by clicking the button of each mode along with the user selecting the time corresponding to each operating process. As data is interchanged during the simulation, the amount of change in power generation, the heat loss and efficiency of the TES tank are calculated in real-time, and the results are shown in the Excel interface as a chart.

2. Performance Analysis

Fig. 9 shows the variation of power generation by IP ST and LP ST for three hours charging and six hours discharging when the normal and saving time is nine hours and six hours accordingly. As a base case, we employed an operation time of three hours for charging, six hours for storing, eight hours for discharging and seven hours for normal mode as summarized in Table 7. During charging mode, 39.3 MW of thermal energy was stored in the TES tank. During discharge, 7.3 MW of thermal energy was released to

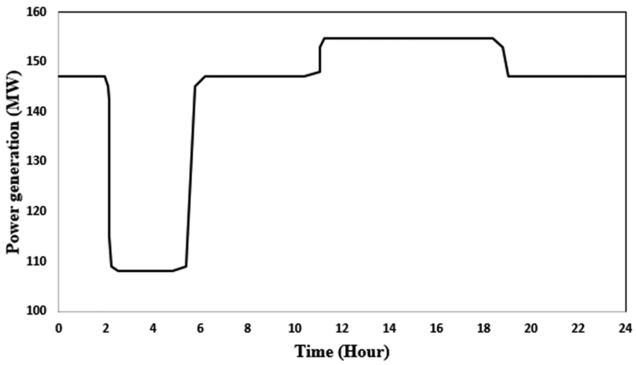

Fig. 9. Various power generation of IP and LP ST for four modes based on daily power.

LP ST by the TES tank. In conclusion, the average TES efficiency was 99.66%.

The mass balance of the two-tank TES with a CC is presented for four operational modes in Tables 5 and 6 based on Fig. 2. Table 5 shows the heat and material balance of the two-tank TES in storing/normal mode. Since TES is disconnected from the CC (see Fig. 4(b)), both modes share the same heat and material balance. These modes correspond to the normal operation of a CC without TES. However, there is a difference in view of TES. While the storing mode saves thermal energy in TES through the charging

Table 5. Heat and material balance of combined cycle with TES system for storing or normal operational mode

Stream No.	1	2	3	4	5	6
Description	From GT	From IP RH	To IP ST	From IP ST	To LP ST	To Stack
Temperature (K)	876.0	838.9	838.9	525.3	525.2	418.2
Pressure (KPa)	104.8	2,302.8	2,302.8	241.3	231.3	97.8
Flow rate (kg/s)	592.8	126.3	126.3	116.9	116.9	592.8
Mole Comp						
O_2	0.12	0	0	0	0	0.12
N_2	0.73	0	0	0	0	0.73
CO_2	0.04	0	0	0	0	0.04
H_2O	0.11	1	1	1	1	0.11

Table 6. Heat and material balance of combined cycle with TES system for charging and discharging operation mode

		TES								
Operation mode	Stream No.	A1	A2	A3	A4	A5	A6	A7	A8	5A
	Description	From IP RH	To LP ST	From Cold tank	To Hot tank	From IP ST	To LP ST	From Hot tank	To Cold tank	To LP ST
Charging	Temperature (K)	838.5	518.7	550.0	830.0	n/a	n/a	n/a	n/a	521.2
	Pressure (KPa)	2,302.7	241.3	107	107	n/a	n/a	n/a	n/a	231.3
	Flow rate (kg/s)	60.6	60.6	94	94	n/a	n/a	n/a	n/a	116.9
	Mole Comp									
	H_2O	1	1	0	0	1	1	0	0	1
	TSM	0	0	1	1	0	0	1	1	0
Discharging	Temperature (K)	n/a	n/a	n/a	n/a	524.2	580.2	800.0	550.0	580.2
	Pressure (KPa)	n/a	n/a	n/a	n/a	231.3	229.6	101	101	229.6
	Flow rate (kg/s)	n/a	n/a	n/a	n/a	116.9	116.9	35	35	116.9
	Mole Comp									
	H_2O	1	1	0	0	1	1	0	0	1
	TSM	0	0	1	1	0	0	1	1	0

mode, the normal mode releases thermal energy through discharging mode.

TES for the charging and discharging modes are shown in Table 6 based on Fig. 2(b). The thermal power stored during charging is 38 MW for hot tank in the CC with TES. In discharging mode, the steam from IP ST obtained thermal energy from TES, which resulted in increasing the outlet steam temperature to LP ST. The thermal power released for the inlet steam to LP ST can be calculated in consideration of the thermal efficiency of the TES tank Table 4.

The total power generation of a reference CC without TES was 466.7 MW [48]. In this study, we assumed GT and HP ST as not connected to the TES system. To evaluate the performance of the TES, the efficiency of IP and LP ST, defined as the ratio of total power generation with TES to the total power generation without TES for 24 hours, was calculated as follows:

$$\varepsilon_t = \frac{1}{t_{day}(P_{IP}+P_{LP})}\sum_j t_j(P_{IP,j}+P_{LP,j})\times 100 \quad (15)$$

where ε_t is the TES efficiency of IP and LP ST, j=charging, storing, discharging and normal mode.

Table 7. Total various power generation and efficiency of combined cycle with thermal energy storage system for four modes

Operation mode	Charging	Storing/normal	Discharging
Operation time	3 hours	6 hours/7 hours	8 hours
GT		272.3 MW	
HP		47.0 MW	
IP+LP	108.1 MW	147.4 MW	154.7 MW
Total	427.4 MW	466.7 MW	474.0 MW
Efficiency		98.31%	

Fig. 10 represents the heat loss results of the molten salt as its level rises in the cold and hot tanks during the charging and discharging modes. With the increasing surface of the wetted area in the two tanks, the heat loss through the side walls consequently increases. Contrarily, the non-wetted area of the tanks reduces, which translates into the heat transfer contribution by radiation. However, since the conduction heat transfer through the bottom of the

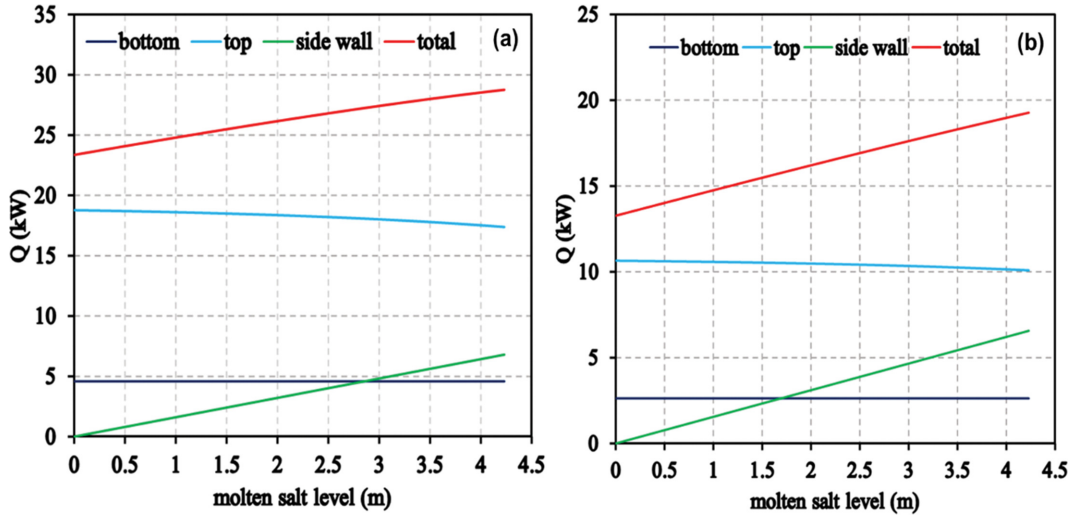

Fig. 10. Heat losses through the different sides of the tanks as the molten salt level increases during filling. (a) 3 h charging time of hot tank, (b) 8 h filling time of cold tank.

tanks is not influenced by the levels of the molten salt, it remains the same at approximate values of 2.6 kW and 4.6 kW for the cold and hot tanks, correspondingly. The trend shown by the curves in the figure above is of close agreement with the results of Schulte-Fischedick et al. [52] while the difference in values can be attributed to geometry used. This was expected because the hot tank is at a higher temperature than the cold tank. The contrasting effects of heat loss contributions through the top and the side walls of the tanks nearly gave constant overall heat loss. The three hour charging of the hot tank at a flowrate of 94 kg/s slightly increased in heat loss from 23.4 kW to 28.8 kW while that of the cold tank increased from 13.3 kW to 19.3 kW for 8 h filling time at a flowrate of 35 kg/s. Hence, heat loss of approximately 48 kW is incurred during the charging/discharging mode of CC with TES which is 0.01% of the total power produced by the plant.

Fig. 11 shows the molten salt cool down curves for both hot and cold tanks at full load. From the operation strategy of the CC with TES, the storing and normal mode for this study is 6 h, which

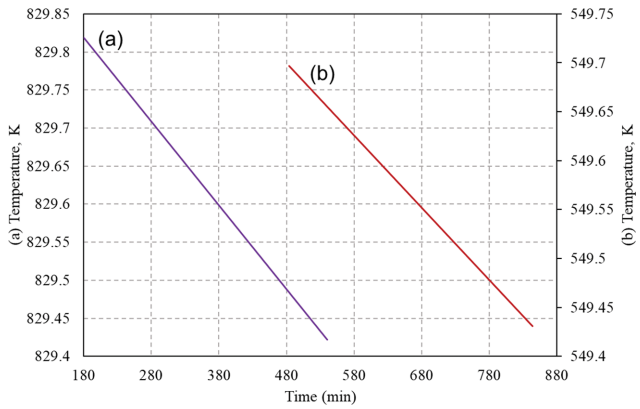

Fig. 11. Molten salt temperature drop of the two-tank thermal energy storage during the 6 h storing/normal mode. (a) Hot tank, (b) Cold tank.

was chosen based on Fig. 1. A short while into these modes, the simulation showed constant temperature difference for the period, which is clearly seen in Fig. 11. The heat loss contribution through the bottom remained constant, while that through the non-wetted and wetted walls showed slight changes.

This is because the level of the molten salt was constant and hence no change in areas for wetted side walls and non-wetted walls. Consequently, hourly temperature drop rates of 0.04 K and 0.06 K with a corresponding approximated heat loss of 19.3 kW and 28.7 kW were obtained in these operation modes for the cold and hot tanks. With the heat loss rate in the two tanks, an average efficiency of 99.95% can be expected for the duration in the storing and normal modes.

For the entire operation modes, the study obtained efficiencies of 99.69% for the cold tank at a temperature drop rate of 0.1 K and 99.63% for the hot tank with 0.18 K cool down rates. More energy was lost during discharge followed by the storing mode. The charging mode contributed the least to heat loss.

However, the heat loss rate during discharge was higher for the cold than the hot tank. This was as a result of the differences in the molten salt flow rates. A similar trend was observed in the charging mode for the two tanks that are higher flow rates yielded more heat loss.

3. Parametric Study and Thermodynamic Analysis

Three case studies on discharging time of TES were conducted

Table 8. Parametric study and efficiency analysis of different operation modes depend on discharging operating time within different flow rate from hot tank to cold tank

Operating time (h)	Case 1	Case 2	Case 3
Charging	3	3	3
Storing	6	6	6
Discharging	6	8	10
Normal	9	7	5
Efficiency	98.1%	98.3%	98.5%

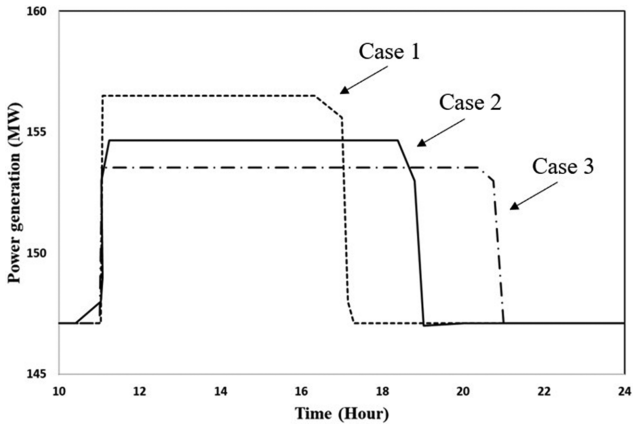

Fig. 12. Power generation of IP and LP ST with TES based on three different discharging times (Case 1: 6 hour discharging, case 2: 8 hour discharging, case 3: 10 hour discharging).

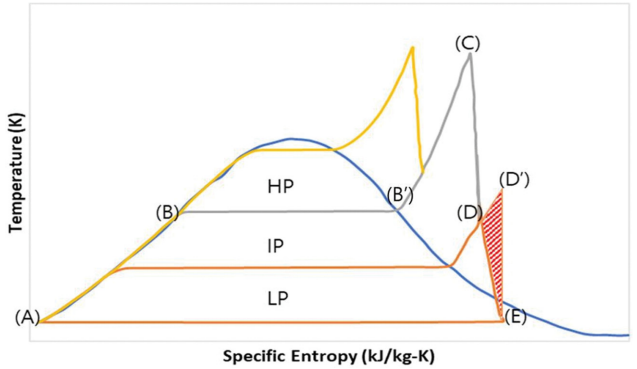

Fig. 13. T-S diagram of Rankine cycle: line (A)-(B)-(C)-(D)-(E) is CC without TES at the various operation modes while line (A)-(B)-(C)-(D)-(D′)-(E) is CC with TES at only discharging mode.

in reference to the daily power demand shown in Fig. 1. To effectively deal with the irregular peak load demand and understand the performance of the TES system, dynamic simulation at varying discharge time was carried out and the results are summarized in Table 8.

The power generation was 156.4 MW, 154.7 MW, and 153.9 MW for the three cases. Corresponding efficiencies using Eq. (15) were computed obtaining 98.10%, 98.30% and 98.50%. These results as Fig. 12 and Table 8 display imply that with a small loss of efficiency, the operation time for discharging can be flexibly adjusted according to power demand. Finally, the power generated in the three cases as illustrated in Fig. 9 give an insight into the behavior of the TES system during discharging mode.

Fig. 13 shows a T-S diagram of the Rankine cycle with three-stage ST consisting of HP, IP and LP.

The main characteristics of the T-S diagram are as follows [43]:

- Process (A)-(B): Water is heated at the economizer in HRSG. The details of this step are captured in Fig. 2(a).
- Process (B)-(C): The line (B)-(B′) is for phase change from liquid water to vapor. (B′) is the saturation point. This step occurred at the LP, IP, and HP steam boiler in Fig. 2(a). The line from (B) to (C) describes the superheating process of water vapor.
- Process (C)-(E)-(A): There are two routes for this process: (C)-(D)-(E)-(A) for charging and storing/normal mode and (C)-(D)-(D′)-(E)-(A) for discharging mode. As discussed, the former corresponds to a T-S diagram for a conventional Rankine cycle. Line (C)-(D) denotes the process from IP RH to LP ST. The IP steam generated the power at IP ST and the exhaust steam was sent to LP ST, which corresponds to streams 3, 4 and 5 in Table 5. Line (D)-(E) represents the step from LP ST to condenser and power generation at LP ST during charging or storing/normal mode as demonstrated in Fig. 7(a) and (b). This is also the case even for a conventional ST.

However, careful attention should be made to the process (D)-(D′)-(E) since this explains the additional power generation during the discharging model with TES. Point (D′) means the LP steam was reheated in the discharging mode and the temperature rose accordingly. This situation was quantified in Table 6 through stream A5 and A6 in this paper. The area with red stripes is the driving force to increase the power generation by supplying thermal energy from TES during discharging mode. The principle used in this study can be employed when HP ST relates to TES in a CC.

- Process (E)-(A): This process explicated the steam flow from LP ST to HRSG, and the vapour was condensed into liquid water.

As a result, a T-S diagram allowed a qualitative thermodynamic interpretation for TES with a CC. From the observation of Fig. 13, TES is applicable not only with a CC but also with other power generation plants, such as CSP and NPP, when operation and design conditions are satisfied.

CONCLUSION

The study explored the feasibility of integrating a combined cycle power plant with a TES system. This is relevant to meeting the varying daily demand for electricity by utilizing an existing power generation plant. To this purpose, a multiscale model was developed whereby TES was integrated to augment the energy production of CC during the higher demand by storing energy at low demand of power, as shown in Fig. 3. The transient behavior of the integrated system was simulated with SimCentral to ascertain the performance and usefulness of TES. While SimCentral does well to provide process insight into the entire plant, it was necessary to assess the effectiveness of the two-tank TES system in terms of energy loss. SimCentral could not provide those details because its models are black-box type. In this light mesoscale two-tank TES was modeled with gPROMS which was coupled with SimCentral using a developed excel interface in this research. That ensured communication between the macroscale model of CC and the mesoscale model of the two-tank TES for the dynamic simulation and time synchronization.

The power generated by the CC without TES was 466.7 MW, which was reduced to 427.4 MW when the TES was set online in charging. This in effect increased the power production to 474.0 MW when the energy stored in the TES system was released to the steam turbines. It implies that the 3-hour charging of the TSM caused the CC to lose 39.3 MW of power; however, 7.3 MW was

added to its original production capacity after 8-hour discharge of the TSM energy to the steam stream. Also, we conducted a parametric study on different discharging times of the TSM to get an insight into the varying daily demand for electric power. In the analysis, discharging times of 6 and 10 hours generated additional power of 9.0 MW and 6.5 MW, respectively. Comparing the CC integration with TES to CC only, the maximum efficiency obtained was 98.5% and the minimum was 98.1%.

Through this study, we have successfully integrated the macroscale combined cycle power plant and the mesoscale TES system. The dynamic simulation results of the presented detailed mathematical model were validated. The methodology of this research finding could present a research direction of processes requiring coupling of various model scales between different computational tools, such as detailed nuclear reactor design and integration processes in chemical engineering.

ACKNOWLEDGEMENTS

This work was supported by the Industrial Strategic Technology Development Program-Engineering Core Technology Development Project (Project No. 201703220003, Development of basic design and FEED automation task support system based on Cloud system) funded By the Ministry of Trade, Industry & Energy (MOTIE, Korea).

NOMENCLATURE

A	: area [m^2]
C_p	: heat capacity [kJ/K]
ε	: emissivity
h	: heat transfer coefficient [$Wm^{-2}K^{-1}$]
h_{in}	: inlet specific enthalpy [kJ/kg]
h_{out}	: outlet specific enthalpy [kJ/kg]
k	: thermal conductivity [$Wm^{-1}K^{-1}$]
m	: mass [kg]
m_{in}	: inlet mass flowrate [kg/s]
m_{out}	: outlet mass flowrate [kg/s]
q	: energy [kJ]
R	: heat transfer resistance
r	: radius [m]
T	: temperature [K]
t	: time [s]
V	: volume [m^3]
ρ	: density [kg/m^3]
σ	: Stefan Boltzmann constant [$kgs^{-3}K^{-4}$]
x	: n dimensional vectors of variables
y	: m dimensional vectors of variables
x′	: derivative of x with respect to t
f	: n dimensional systems of equation
g	: m dimensional systems of equation
h_n	: integration step length
α_k, β_k	: BDF coefficient
$\gamma_{k,n}$	: accumulation of past history terms in the BDF method

Abbreviations

CC	: combined cycle
TES	: thermal energy storage
CHP	: combined heat and power
CSP	: concentrating solar power
PCM	: phase change material
NPP	: nuclear power plants
IGCC	: integrated gasification combined cycle
NGCC	: natural gas combined cycle
NPP	: nuclear power plants
SHS	: sorption heat storage
ModDev	: model development
MoT	: modeling tool
HRSG	: heat recovery steam generator
TSM	: thermal storage material
GT	: gas turbine
ST	: steam turbine
LP ST	: low pressure steam turbine
IP ST	: intermediate pressure steam turbine
HP ST	: high pressure steam turbine
HP ST	: heat exchanger

Superscript

d	: conduction
γ	: radiation
v	: convection

Subscript

b	: bottom
i, j	: nodes
l	: lateral side
rf	: roof

REFERENCES

1. M. Khanna and M. D. Rao, *Annu. Rev. Resour. Econ.*, **1**, 568 (2009).
2. M. Johnson, J. Vogel, M. Hempel, A. Dengel, M. Seitz and B. Hachmann, *Energy Procedia.*, **73**, 281 (2015).
3. Interactive Gas Turbine Portfolio Brochure, Siemens, https://assets.new.siemens.com/siemens/assets/api/uuid:10f4860b140b2456f05d32629d8d758dc00bcc30/gas-turbines-siemens-interactive.pdf.
4. A. Rahman, A. D. Smith and N. Fumo, *Appl. Therm. Eng.*, **100**, 668 (2016).
5. C. A. Cruickshank, *Evaluation of a stratified milti-tank thermal storage for solar heating applications*, PhD Thesis, Queen's University (2009).
6. I. Rodríguez, C. D. Pérez-Segarra, O. Lehmkuhl and A. Oliva, *Appl. Energy*, **109**, 402 (2013).
7. I. L. Garcia, J. L. Alvarez and D. Blanco, *Sol. Energy*, **85**, 2443 (2011).
8. C. Parrado, A. Marzo, E. Fuentealba and A. G., Fernandez, *Renew. Sustain. Energy Rev.*, **57**, 505 (2016).
9. L. Heller and P. Gauche, *Sol. Energy*, **93**, 345 (2013).
10. C. Daniel, S. Natalie and F. Charles, *Trans. Amer. Nucl. Soc.*, **116**(2), 837 (2017).
11. J. Edwards, H. Bindra and P. Sabharwall, *Ann. Nucl. Energy*, **96**, 104 (2016).
12. O. Maurstad, LFEE, 2005-002 WP (2005), https://sequestration.mit.edu/pdf/LFEE_2005-002_WP.pdf.

13. B. J. Alqahtani and D. Patiño-Echeverri, *Appl. Energy*, **169**, 927 (2016).
14. O. Garbrecht, M. Bieber and R. Kneer, *Energy*, **118**, 876 (2017).
15. M. Johnson, J. Vogel, M. Hempel, A. Dengel, M. Seitz and B. Hachmann, *Energy Procedia*, **73**, 281 (2015).
16. P. Verma, Varun and S. K. Singal, *Renew. Sustain. Energy Rev.*, **12**(4), 999 (2008).
17. V. Vasilios, US Patent, 61,954,619 (2014).
18. K. Drost, Z. Antoniak and D. Brown, *Energy Conv. Eng. Con.*, **4**, 251 (1990).
19. M. K. Drost, Z. I. Antoniak, D. Brown and S. Somansundaram, US. Dep. Energy, PNL-7403 (1990).
20. W. Q. Tao and Y. L. He, IHTC 14. 8, 671 (2010), https://doi.org/10.1115/IHTC14-23408.
21. V. V. Krzhizhanovskaya, D. Groen, B. Bozak and A. G. Hoekstra, *Procedia. Comput. Sci.*, **51**, 1082 (2015).
22. A. Helmns and V. P. Carey, *J. Therm. Sci. Eng. Appl.*, **10**(5), 051004 (2018).
23. M. Parsazadeh and X. Duan, *Appl. Energy*, **216**, 142 (2018).
24. M. Fasano, D. Borri, A. Cardellini, M. Alberghini, M. Morciano, E. Chiavazzo and P. Asinari, *Energy Procedia*, **126**, 509 (2017).
25. J. C. Lee, O. S. Kofi, S. Y. Kim, S. G. Hong and M. Oh, *J. Eng. Sci. Technol.*, **10**, 48 (2015).
26. R. Morales-Rodriguez and R. Gani, *Comput. Aided Chem. Eng.*, **24**, 207 (2007).
27. R. Morales-Rodríguez and R. Gani, *Comput. Aided Chem. Eng.*, **26**, 495 (2009).
28. R. Morales-Rodríguez, R. Gani, S. Déchelotte, A. Vacher and O. Baudouin, *Chem. Eng. Res. Des.*, **86**, 823 (2008).
29. Z. Jaworski and B. Zakrzewska, *Comput. Chem. Eng.* **35**(3), 434 (2011).
30. P. Heidebrecht, M. Pfafferodt and K. Sundmacher, *Chem. Eng. Sci.*, **66**(19), 4389 (2011).
31. D. G. Vlachos, A. B. Mhadeshwar and N. S. Kaisare, *Comput. Aided Chem. Eng.*, **30**(10-12), 1712 (2006).
32. G. Pozzetti and B. Peters, *Int. J. Multiph. Flow.*, **99**, 186 (2018).
33. H. M. Park, *Int. J. Heat Mass Transf.*, **75**, 545 (2014).
34. D. H. Oh, R. Y. Jeon, J. H. Kim, C. H. Lee, M. Oh and K. J. Kim, *Cryst. Growth Des.*, **19**(2), 658 (2019).
35. N. D. Vo, M. Y. Jung, D. H. Oh, J. S. Park, I. Moon and M. Oh, *Combust. Flame*, **189**, 12 (2018).
36. G. H. Lee, N. D. Vo, R. Y. Jeon, S. W. Han, S. U. Hong and M. Oh, *Korean J. Chem. Eng.*, **35**(9), 1791 (2018).
37. H. H. Lee, J. C. Lee, Y. J. Joo, M. Oh and C. H. Lee, *Appl. Energy*, **131**, 425 (2014).
38. Electrical energy storage, Technical Report, International Electrochemical Commission, http://www.iec.ch/whitepaper/pdf/iecWP-energystorage- LR-en.pdf (2011).
39. E. Weinan, B. Engquist, X. Li, W. Ren and E. Vanden-Eijnden, *Commun. Comput. Phys.*, **2**(3), 367 (2007).
40. G. D. Ingram, I. T. Cameron and K. M. Hangos, *Chem. Eng. Sci.*, **59**(11), 2171 (2004).
41. J. O. Dada and P. Mendes, *Integr. Biol.*, **3**(2), 86 (2011).
42. A. Yang and W. Marquardt, *Comput. Chem. Eng.*, **33**(4), 822 (2009).
43. A. Hoekstra, B. Chopard and P. Coveney, *Philos. Trans. R. Soc. A Math. Phys. Eng. Sci.*, **372**(2021), 20130377 (2014).
44. B. Chopard, J. Borgdorff and A. G. Hoekstra, *Philos. Trans. R. Soc. A Math. Phys. Eng. Sci.*, **372**(2021), 20130378 (2014).
45. S. E. Zitney, CAPE-OPEN integration for advanced process engineering co-simulation, Final Report. DOE/NETL-IR-2007.
46. F. Zaversky, J. García-Barberena, M. Sánchez and D. Astrain, *Sol. Energy*, **93**, 294 (2013).
47. R. B. Jarvis and C. C. Pantelides, *Robust dynamic simulation of chemical engineering processes*, PhD Thesis, Imperial College London University (1993).
48. W. Shelton and J. Lyons, *Shell gasifier IGCC base cases*, Report. NETL PED-IGCC-98-002 (2000).
49. T. E. Boukelia, M. S. Mecibah, B. N. Kumar and K. S. Reddy, *Energy*, **88**, 292 (2015).
50. R. I. Dunn, P. J. Hearps and M. N. Wright, *Proc. IEEE*, **100**(2), 504 (2012).
51. W. S. Lee, J. C. Lee, H. T. Oh, S. W. Baek, M. Oh and C. H. Lee, *Energy*, **134**, 731 (2017).
52. J. Schulte-Fischedick, R. Tamme and U. Herrmann, *Ameri. Soc. of Mech. Eng.*, **2**, 515 (2008).